Novel nanocomposites based on poly(ethylene- co -vinyl acetate) for coating applications: The complementary actions of hydroxyapatite, MWCNTs and ammonium polyphosphate on flame retardancy

Henri Vahabi, Fatemeh Gholami, Valeriia Karaseva, Fouad Laoutid, Rémy Mangin, Rodolphe Sonnier, Mohammad Reza Saeb

Novel nanocomposites based on poly(ethylene-*co*-vinyl acetate) for coating applications: The complementary actions of hydroxyapatite, MWCNTs and ammonium polyphosphate on flame retardancy

Henri Vahabi[a,*], Fatemeh Gholami[b], Valeriia Karaseva[c], Fouad Laoutid[c], Rémy Mangin[a], Rodolphe Sonnier[d], Mohammad Reza Saeb[e,*]

[a] *Université de Lorraine, Laboratoire MOPS E.A. 4423, Metz F-57070, France*
[b] *School of Materials and Mineral Resources Engineering, Engineering Campus, Universiti Sains Malaysia, 14300 Nibong Tebal, Pulau Pinang, Malaysia*
[c] *Laboratory of Polymeric and Composite Materials, Materia Nova Research Center, Avenue Copernic 1, 7000 Mons, Belgium*
[d] *Centre des Matériaux des Mines d'Alès (C2MA)-6, Avenue de Clavières, 30319 Alès Cedex, France*
[e] *Department of Resin and Additives, Institute for Color Science and Technology, P.O. Box: 16765-654 Tehran, Iran*

A B S T R A C T

Nowadays, researchers working in the realm of coating or related industries are expected to propose novel materials with multifunctional capabilities. In this work, novel nanocomposites based on poly(ethylene-*co*-vinyl-acetate) (EVA) copolymer, hydroxyapatite (HA), carbon nanotubes (CNTs) and ammonium polyphosphate (APP) are proposed and examined for thermal stability and flammability. Thermogravimetric analysis and cone calorimeter tests evidenced that HA/CNTs combination presents a promising effect on both thermal and flame retardancy behavior of EVA. Cone calorimeter results approved in a similar manner that the incorporation of only 5 wt.% HA-CNTs into the EVA significantly drops peak of heat release rate (pHRR) (around 37%). The flame retardant effect was further improved when HA or HA-CNTs were associated with APP. The pHRR decreased by 76–77% for EVA containing HA or HA-CNTs and APP compared to the neat EVA. The performance of developed nanocomposites was compared with more than 100 flame retardant systems previously reported in the literature.

Keywords:
Poly(ethylene-*co*-vinyl acetate)
Flame retardancy
Hydroxyapatite
Thermal degradation
Carbon nanotube

1. Introduction

Poly(ethylene-*co*-vinyl acetate) (EVA) is a copolymer widely practiced in various applications such as construction, electrical cable and wire coating, packaging, adhesive, solar energy, agriculture, and sports [1–3]. The global EVA production is approximately 5 million tons per year. Its global market is expected to grow at a Compound Annual Growth Rate (CAGR) of 5.14% during the period 2016–2020 [4]. In the form of latex, EVA can be applied in coatings applications when its solid content is high and its viscosity is sufficiently low [5]. For instance, the blend of EVA with polyethylene and ethylene vinyl alcohol was applied as coating, where varying the concentration of iron oxide and titanium oxide pigments [6]. The resulting composites were sprayed on mild steel and good mechanical and anticorrosive properties were achieved. Furthermore, for some applications the flame resistant character of coating is needed in order to protect the underlying material. For example, in cable industry, NFC 32070 CR1 standard test imposes that cables sustain electrical power where jacket coating protect the copper against heat and fire [7,8]. In this case, coating plays an important role on fire protection during the combustion by decreasing the heat transfer from the surface to the underlying substrate [9,10].

Despite promising aspects of EVA which makes it a candidate for coating applications, it is highly flammable. The incorporation of flame retardant additives into the EVA is a well-known way to improve its low fire resistance. The effect of diverse flame retardants on the flammability of EVA has already been investigated [11–22]. During recent years, researchers fascinatingly tested the combination of conventional flame retardants like phosphorous ones with mineral fillers and/or nanoparticles. The connectivity, thickness and porosity of the char remained from combustion as well as its dimensional expansion as an integrated layer could be attributed to the improvement of flame retardancy [23–25]. Therefore, the use of phosphorous flame retardants like ammonium polyphosphate (APP) in combination with mineral nanoparticles of different nature such as montmorillonite [26,27], zeolite [28], MgO [29], expandable graphite [30], expanded graphite [31], layered double hydroxides (LDH) [32], $CaCO_3$ [31] in EVA has been reported by several authors.

Application of green or environmental-friendly substances in

* Corresponding authors.
E-mail addresses: henri.vahabi@univ-lorraine.fr (H. Vahabi), saeb-mra@icrc.ac.ir, mrsaeb2008@gmail.com (M.R. Saeb).

polymer systems has become a necessity nowadays. In this sense, incorporation of hydroxyapatite ($Ca_5(OH)(PO_4)_3$) (HA) into several polymers such as poly(methyl methacrylate) (PMMA), polycarbonate (PC), polyester and epoxy resin was carried out for the sake of higher flame retardancy [33–35]. The HA is a bio-based polycrystalline calcium phosphate ceramic in a hexagonal form with 39 wt.% of Ca, 18.5 wt.% of P and 3.38 wt.% of OH. The effect of incorporation of HA on EVA mechanical properties has already been reported [36–38]. Because of its merit, it has been mostly applied in medical applications, but, to the best of the knowledge of the authors of this work, it has not been used for increasing fire resistance of EVA. There are also some reports showing that the use of carbon nanotubes (CNTs) enhances the flame retardancy character of EVA [39–44].

In the light of above, combined use of HA and CNTs could have been responsible for achieving an innovative EVA nanocomposites with flame retardant properties. In the present work, the effect of HA alone, the physical blend of HA and multi-walled CNTs (hereinafter referred to as HA-CNTs), the blend of APP and HA (APP/HA), and eventually APP/HA-CNTs on thermal behavior and flame retardancy of EVA was thoroughly discussed. The HA and HA-CNTs were synthesized through precipitation method and characterized by scanning electron microscopy (SEM), transmission electron microscopy (TEM), Fourier transform infrared spectroscopy (FTIR), and X-ray diffraction (XRD) analyses. A series of EVA nanocomposites containing one or combination of two or three aforementioned components were prepared and characterized for thermal stability and flame retardancy by thermogravimetric analysis (TGA) and cone calorimetry measurements. The synergistic effects of the used ingredients on flame retardant properties was discussed and compared with more than 100 classes of flame retardants based on EVA.

2. Materials and methods

Poly(ethylene-*co*-vinyl acetate), EVA, (Escorene TM Ultra FL00014; MFI = 0.25 g/10 min and vinyl acetate rate = 14%) was provided by ExxonMobil. Ammonium polyphosphate (APP), Exolit AP423, was purchased from Clariant. $Ca(NO_3)_2{\cdot}4H_2O$ (> 99%), $(NH_4)_2HPO_4$ (> 98%), NH_4OH (28–30%) were obtained from Sigma-Aldrich, Malaysia. MWCNT (DI = 20–30 nm, L = ≈30 μm, 99.9%) were supplied by the Chinese Academy of Science. These reagents were used without further purification for this study.

2.1. Synthesis of hydroxyapatite (HA) and hydroxyapatite/multiwalled carbon nanotubes (HA-CNT)

HA was prepared by precipitation technique with $Ca(NO_3)_2{\cdot}4H_2O$ and $(NH_4)_2HPO_4$ as starting materials and ammonia solution (NH_4OH) to control pH during the process. A solution of 0.24 M $Ca(NO_3)_2{\cdot}4H_2O$ (350 mL) was stirred vigorously, and the temperature was kept at 30 °C (± 3 °C). A solution of 0.29 M $(NH_4)_2HPO_4$ (250 mL) was added dropwise into the $Ca(NO_3)_2{\cdot}4H_2O$ solution. Throughout the experiment, the pH was kept above 10.5 (10.5–11) by infinitesimal addition of ammonia solution. Nanosized powder of HA was hydrothermally synthesized based on the following reaction:

$$10Ca(NO_3)_2 + 6(NH_4)_2HPO_4 + 8NH_4OH = Ca_{10}(PO_4)_6(OH)_2 + 20NH_4NO_3 + 6H_2O$$

During the precipitation, the solution was stirred, and the final suspension was continuously stirred for 6 h after the remaining part of the $(NH_4)_2HPO_4$ solution was added. In the next step, the resulting suspension was covered and left to age at room temperature for 24 h. After ageing, the precipitated HA was removed from the solution by centrifugation (rotation speed of 4000 rpm). The resultant powder was dried at 80 °C overnight and subsequently calcined at 800 °C for 2 h.

Ultrasonication was served for mixing through which HA-CNT powder was prepared. The HA powder was added to ethanol and mixed with a magnetic stirrer for 30 min. The powder was dispersed ultrasonically to obtain a homogeneous suspension. MWCNTs (CNT) powder was added to the suspension of HA powder (in a ratio of 1:20 by wt.%) and ultrasonically mixed for 3 h. The HA-CNT was allowed to dry in air at room temperature for 24 h.

Table 1
Name and composition of all samples.

Sample code	EVA (wt.%)	HA (wt.%)	HA-CNT (wt.%)	APP (wt.%)
EVA	100	0	0	0
EVA/HA	95	5	0	0
EVA/HA-CNT	95	0	5	0
EVA/APP	80	0	0	20
EVA/APP/HA	80	5	0	15
EVA/APP/HA-CNT	80	0	5	15

2.2. Composite preparation

Blending of the different additives within the molten EVA was carried out in a Brabender internal mixer at 180 °C (3 min mixing at 30 rpm prior to 7 min mixing at 60 rpm). The compositions of the prepared blends are presented in Table 1. The samples were then grinded and hot-molded, using an Agila PE20 hydraulic press, under 60 bar for 5 min at 190 °C in order to obtain square sheets of 100 × 100 × 4 mm^3.

2.3. Characterization

Chemical and physical characterizations of HA and HA-CNT particles were carried out using different techniques including Scanning Electron Microscopy (SEM), Transmission Electron Microscopy (TEM), Fourier Transformed Infrared Spectroscopy (FTIR) and X-ray Diffraction Analysis (XRD). SEM analysis was performed with a Leo Supra 50 VP (Germany) electron microscope and Quanta FEG450 model scanning electron microscope to investigate the microstructure and morphology of the developed particles. Sample fracture fragments were mounted on a conducting carbon tape and analyzed using an accelerating voltage of 5 kV and a secondary electron detector. TEM analysis was carried out to provide deep insights into the morphology and particle size of the materials at the atomic level structure. Phillips electron microscope-CM12 (Philips, Netherlands) provided with an Image Analyzer (Model Soft Imaging System, SIS 3.0) operated at 30 kV. A small amount of powder samples was placed onto a carbon film on copper grid. Fourier transform infrared spectroscopy (FTIR) was used to investigate the functional groups present in the samples using the Perkin–Elmer FTIR 2000 spectrometer. The FTIR spectra were recorded in the wave number interval of 4000 cm^{-1} to 400 cm^{-1} under transmittance mode. The resolution of the spectrometer was 4 cm^{-1}. Before analysis, calibration of the spectrometer was performed with polystyrene as a control sample. The test sample was mixed with potassium bromide with a weight ratio of approximately 1:10. The mixture was ground to a fine, homogeneous powder, which was then poured into a mold. The powder was compacted with a hydraulic press set at 600 MPa pressure to form thin pellets. The resulting pellets were then placed in the sample holder for FTIR analyses. A Siemens D-5000 X-ray diffractometer was used to identify the chemical composition of the crystalline phases in HA an HA-CNT particles. XRD patterns were recorded over a 2θ angle range of 20° to 70° at a sweep rate of 0.04° s^{-1}.

Morphological investigation was also performed to highlight the dispersion state of the additives in EVA using a scanning transmission electron microscopy (STEM) Hitachi SU8020 (100 V–30 kV) apparatus. For SEM observations, EVA composites were cryo-fractured after immersion in liquid nitrogen and then coated using a gold sputtering

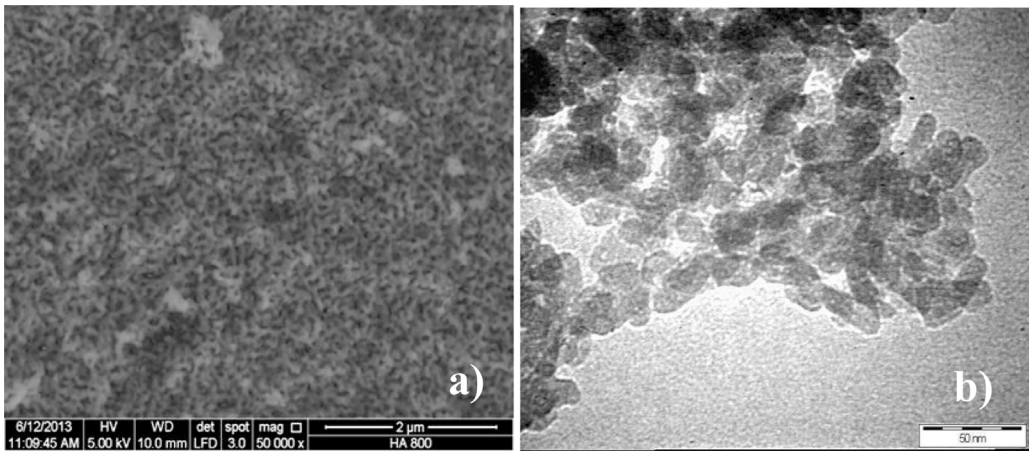

Fig. 1. SEM (a) and TEM (b) images of synthesized HA.

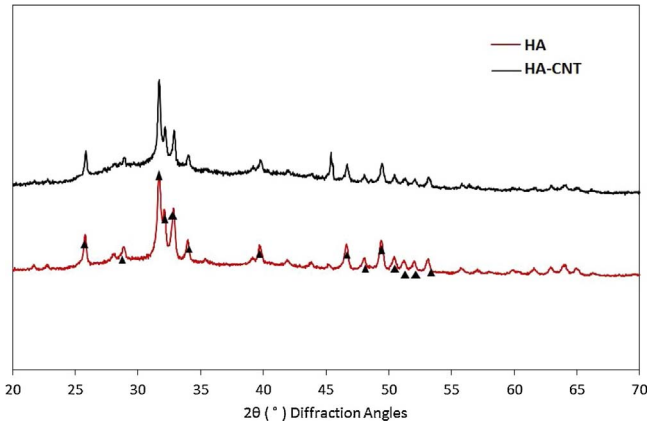

Fig. 2. X-ray diffraction patterns of HA and HA-CNT.

technique to avoid any charging effect during the electron beam scanning. Thermal gravimetric analysis (TGA) was performed on a Setaram Labsys Evo thermogravimetric analyzer at a heating rate of 10 °C min^{-1}. The samples of approximately 20 mg were introduced in TGA Labsys Evo alumina crucible, and analyzed under a nitrogen flowing rate of 50 mL min^{-1} and at temperatures ranging from room temperature to 700 °C. A cone calorimeter (Fire-EU-ISO5660) was used to assess the fire behavior of the samples. The procedure used involves exposing specimens at heating flux levels of 35 kW m^{-2}. The parameters measured were Heat Release Rate (HRR), Time-To-Ignition (TTI), Total Heat Release (THR), Total Smoke Production (TSP), and Effective Heat of Combustion (EHC) and residue content. For each sample, the test was performed three times and the experimental error was around 5%.

3. Results and discussion

3.1. Characterization of HA and HA-CNT

Fig. 1 presents SEM (a) and TEM (b) images of the collected powder. These images evidence the presence of nanometric particles with uniform structure (from 20 to 50 nm).

The structure of these nanoparticles has been investigated by using X-ray diffraction as well as Fourier transform infrared spectroscopy (FTIR). X-ray patterns of HA and HA-CNT nanoparticles are presented in Fig. 2. The peak positions are matching closely the diffraction peaks of stoichiometric HA [45]. The crystalline peaks of hydroxyapatite at 2θ = 25.8° (002), 28.2° (102), 31.7° (211), 33° (300), and 34° (302) exhibit its typical structure. As shown in Fig. 2, no CNT peaks were found in the XRD patterns, indicating that the small volume fraction of CNT introduced into the HA makes hardly possible to be detected within the sensitivity limit of XRD [46,47].

The FTIR results indicate that the main peaks observed in Fig. 3 were PO_4^{3-} and −OH. A stretch band of −OH was observed at 3570 cm^{-1} [48] in the FTIR spectra of synthetic HA powders. PO_4^{3-} (υ3 mode) bands were observed between 1030 and 1050 cm^{-1} and

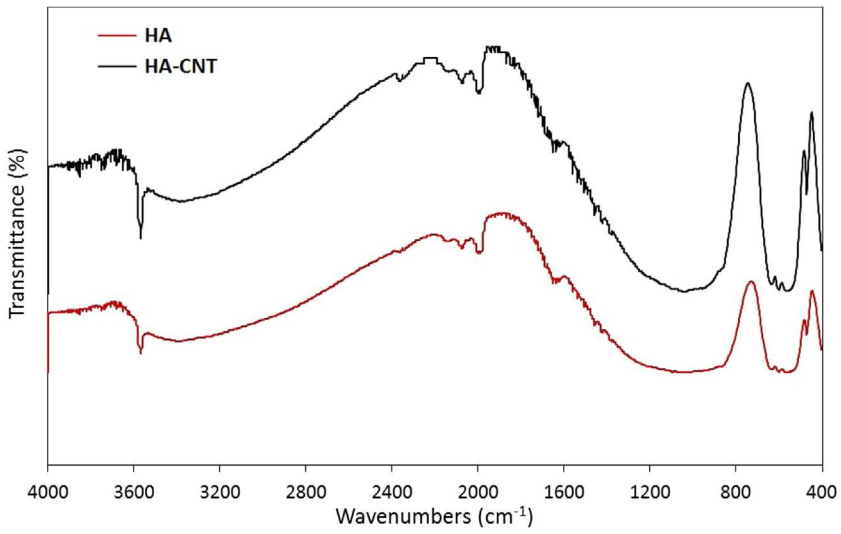

Fig. 3. FTIR patterns of synthesized HA and HA-CNT.

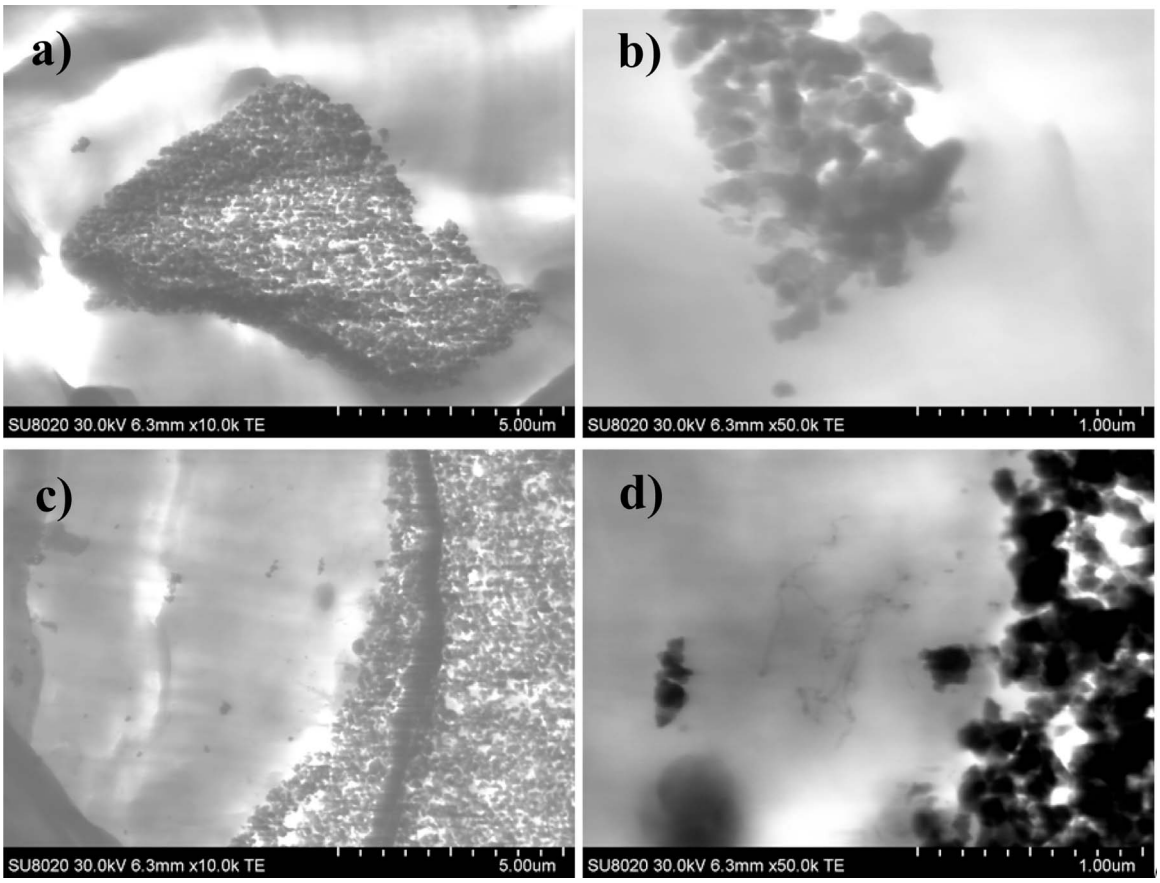

Fig. 4. STEM images of EVA containing HA (a and b) and HA-CNT (c and d).

PO_4^{3-} (υ4 mode) bands between 530 and 571 cm^{-1} [49,50]. These peaks confirm the presence of HA powder. The weak bonds of carbonate in the region ranging from 1380 cm^{-1} to 1620 cm^{-1} were assigned to surface carbonate ions (CO_3^{2-}). Carbonate is an impurity of hydroxyapatite that was originated by CO_2 adsorption from the air during process or starting material [51]. The obtained results confirm the presence of HA powder. Due to the low amount of CNT in HA/CNT blend no obvious peak belonging to the characteristic stretching vibrations of C—C bonds was observed in these FTIR spectra.

3.2. Thermal properties and fire behavior of composites

3.2.1. Dispersion state of the fillers

It is well known that when they are individualized and properly dispersed into polymeric matrices, nanoparticles contribute to the enhancement of properties such as thermal and mechanical properties or flame retardancy [52]. They enable a considerable reduction of the loading rate as the interfacial area between the polymer and the nanofiller is greatly increased. For that reason, we investigated the dispersion state of HA and HA-CNT nanoparticles into EVA. Fig. 4 shows STEM images of EVA containing HA and HA-CNT particles and evidences the nanometric size of HA particles as well as their non-optimal dispersion state. Large aggregates of nanoparticles are observed even when HA is associated with CNT. However, some individual HA and CNT nanoparticles are also present in the composite. The compounding process, therefore, did not allow reaching nano-scale dispersion of HA particles. In order to reduce the tendency of HA nanoparticles to agglomerate, a development of adapted surface modification is needed. This is the subject of an ongoing investigation.

The dispersion state of HA nanoparticles is not further improved when combined with APP. SEM observations (Fig. 5) evidence the presence of some HA nanoparticles aggregates while some of them are agglomerated around APP particles. EDX analysis performed during SEM observations indicates the presence of some calcium and phosphorus rich area (HA/APP agglomerates) while other agglomerates contain only calcium without any trace of phosphorus.

3.2.2. Thermogravimetric analysis (TGA)

Fig. 6 presents the TGA curves of neat EVA and the different composites. Main characteristics are shown in Table 2. As can be observed on DTG curves, Fig. 7, degradation occurred in two steps, namely the loss of the acetic acid and the main degradation step related to decomposition of the unsaturated crosslinked backbone, at approximately 350 and 465 °C. At the beginning of mass loss, only small variations of degradation temperature between pristine EVA and composites have been observed. At 10% weight loss, more differences appeared. Pure EVA presented the highest degradation temperature, at 417 °C. The degradation of pure HA and HA-CNT can be neglected due to the low percentage of these fillers in the matrix and also because of very small degradation rate of these particles [33]. Incorporation of HA or HA-CNT did not significantly impact this degradation. However, the incorporation of nanoparticles enables for the formation of some char that is slightly higher when HA-CNT nanoparticles are used (Table 2). The incorporation of APP triggered some modifications of the composite thermal behavior. In comparison with pristine EVA, all formulations containing APP showed a decrease of about 50 °C of the degradation temperature corresponding to 10% weight loss ($T_{10\%}$). This effect is mainly due to the low decomposition temperature of this flame retardant. In contrast to pristine EVA that degrades without forming any residue, the incorporation of APP enables for increasing the amount of the char up to 11%. When combined with HA and HA-CNT, the amount of the residue is increased up to 20 and 14% respectively. The latter result showed that substitution of a part of APP by HA significantly increased the amount of the final residue.

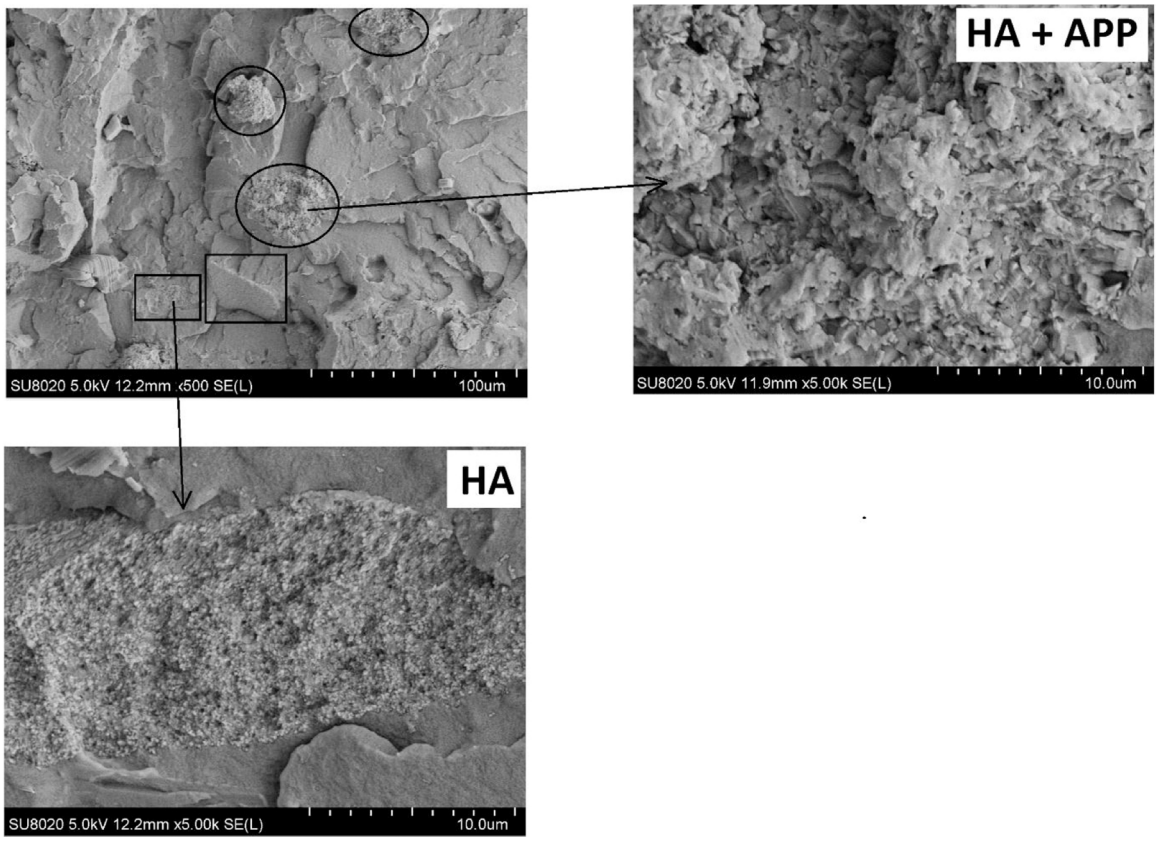

Fig. 5. SEM images of EVA/APP/HA sample.

3.2.3. Cone calorimeter

Fig. 8 shows heat release rate (HRR) curves versus time for EVA and all composites. The corresponding data are summarized in Table 3. EVA was totally burned without leaving any char residue. The peak of HRR (pHRR) of EVA was 905 kW m^{-2} and its time-to-ignition (TTI) was 106 s. Peak of HRR of EVA was decreased upon addition of HA (23%) and HA-CNT (37%). The presence of CNT presents some interest since it enables higher pHRR reduction. However, the shape of these HRR curves did not change in presence of HA or HA-CNT. In contrast, the incorporation of APP, alone or in combination with HA or HA-CNT nanoparticles induces important modification of the burning behavior of the composites. The degree of decrease in pHRR as well as the shape of HRR curve appeared significantly different. The fall in pHRR was 63, 77 and 76% for the EVA/APP, EVA/APP/HA and EVA/APP/HA-CNT sample, respectively. EVA/APP sample presented a high peak at 1000 s. The combination of APP and HA enabled for the reduction of pHRR with respect to the EVA/APP sample. However, the mean of HRR for EVA/APP for 500 s from the beginning of analysis was lower than that

Table 2
TGA parameters for the studied samples.

Sample code	$T_{5\%}$ (°C)	$T_{10\%}$ (°C)	T_{max} (°C)	Residue At 700 °C (wt.%)
EVA	352	417	469	0
EVA/HA	352	407	470	7
EVA/HA-CNT	348	415	468	11
EVA/APP	340	363	469	11
EVA/APP/HA	343	368	466	20
EVA/APP/HA-CNT	343	370	465	14

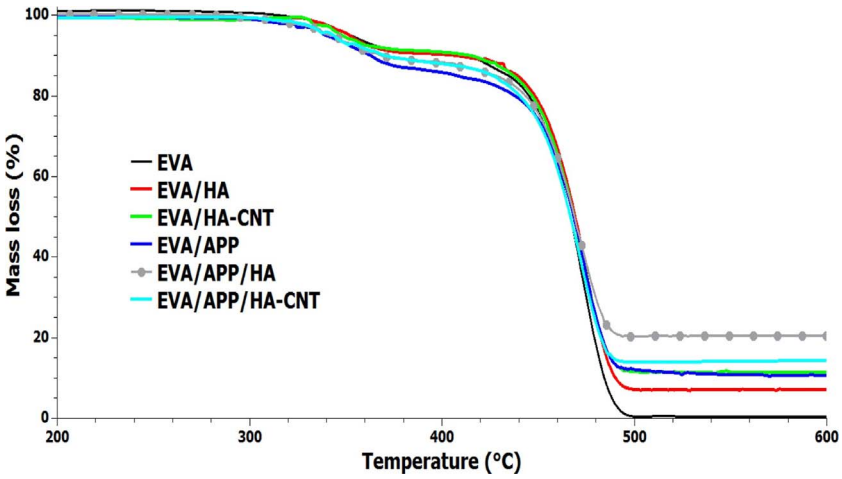

Fig. 6. TGA curves of all samples, at heating rate of 10 °C min^{-1} under nitrogen.

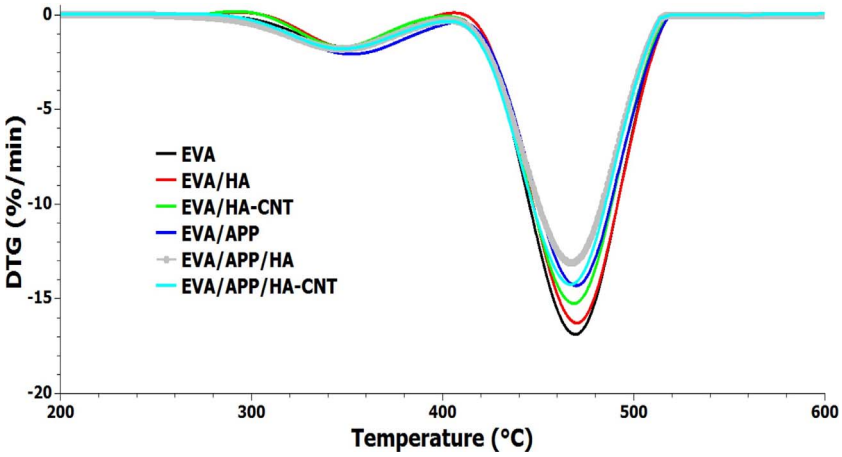

Fig. 7. DTG curves of the studied samples.

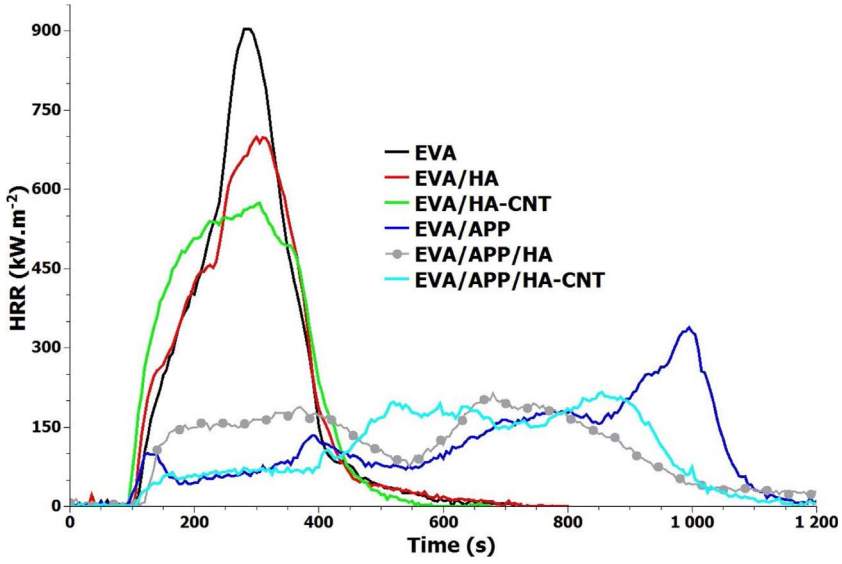

Fig. 8. HRR curves obtained from cone calorimeter test under an incident heat flux of 35 kW $m^{-2.}$

of EVA/APP/HA samples. After 500 s, HRR was progressively increased in the case of EVA/APP sample reaching the value of 335 kW m^{-2} at 1000 s. The presence of CNT did not further reduce pHRR compared to EVA/APP/HA sample. However, the peaks of HRR were shifted to later time in the presence of CNT. Two HRR peaks for EVA/APP/HA sample were observed at 350 and 670 s but registered at 520 and 850 s for EVA/APP/HA-CNT sample (Fig. 8). It can be noticed that the HRR curve of EVA/APP/HA-CNT sample before 400 s showed a plateau around 70 kW m^{-2}. HRR was increased for this sample after 400 s due to the slow and continuous degradation of char barrier during the combustion. Therefore, based on the obtained results in this study, it can be concluded that the reinforcement of this char, through the increasing in HA-CNT content, can provide EVA with further improved flame retardancy.

Even though TTI of EVA/APP/HA was slightly increased, it was not significantly changed for the other samples compared to pristine EVA. The evolution of THR as a function of time is presented in Fig. 9. Two categories of curves can be distinguished from these curves: those of samples containing APP (arrow) and without APP (dashed arrow). EVA/APP/HA-CNT sample presents the smallest value of THR (116 kJ m^{-2}). The comparison of effective heat of combustion (EHC) values, corresponding to the measured heat release divided by the mass loss for a specific time period, are not significantly modified. This result indicates that the flame retardant effect of APP and APP/HA combinations does not affect the chemical composition of the volatiles released but only their amount. Moreover, THR is significantly reduced in the presence of APP showing that the presence of APP amount of the volatiles is strongly limited in the presence of APP-based compositions

Table 3
Summary results of cone calorimetry test, irradiance: 35 kw m^{-2}.

Sample code	pHRR (kW/m^2)	THR (MJ/m^2)	TTI (s)	Residue (%)	EHC (kJ/g)	Reduction in pHRR (%)	TSP (m^2 m^{-2})
EVA	905	153	106	0	40	–	2580
EVA/HA	700	145	101	6	39	23	2220
EVA/HA-CNT	570	147	94	6	39	37	2520
EVA/APP	335	131	96	17	37	63	4370
EVA/APP/HA	212	132	112	15	38	77	3490
EVA/APP/HA-CNT	215	116	106	15	35	76	3580

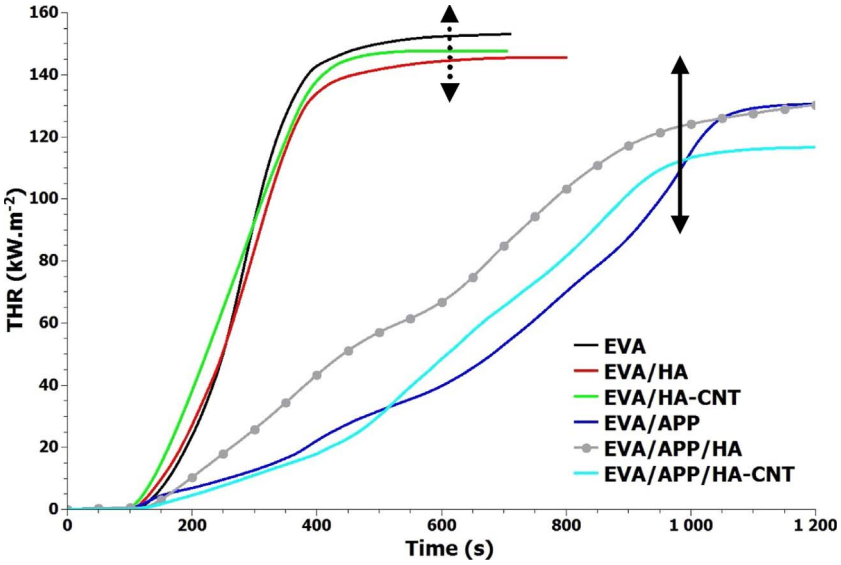

Fig. 9. Total Heat Release as a function of time (Heat flux: 35 kW m^{-2}).

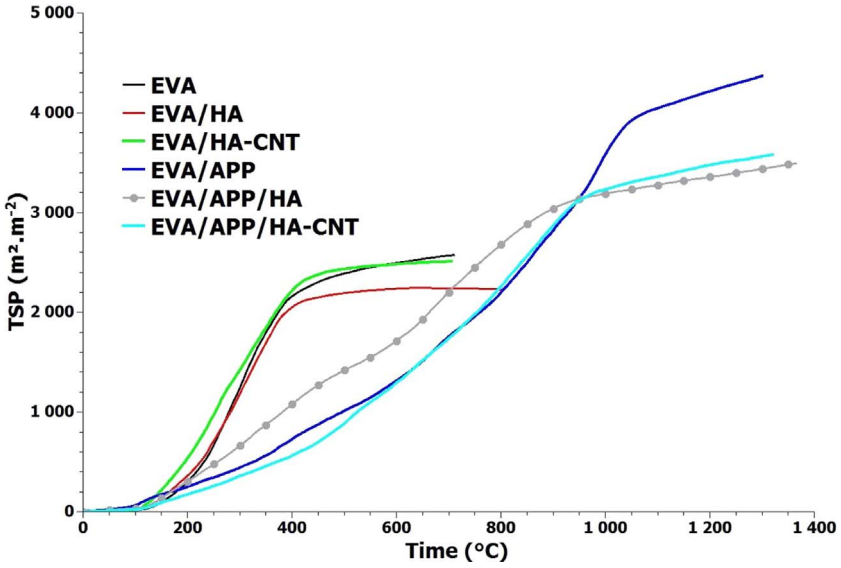

Fig. 10. Total Smoke Production (TSP) curves obtained from cone calorimeter test (Heat flux: 35 kW m^{-2}).

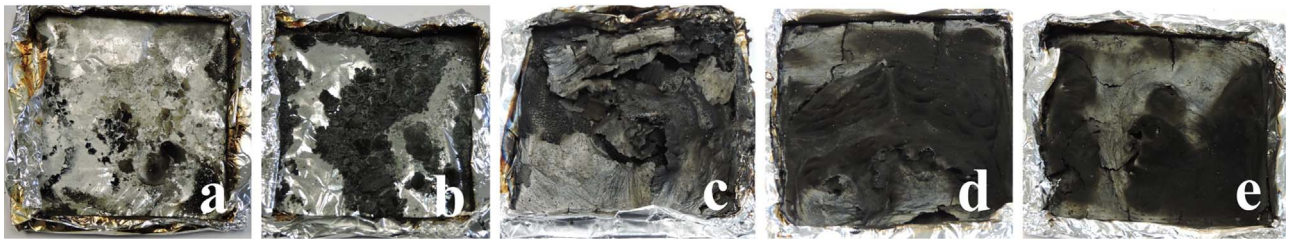

Fig. 11. Photographs of the remaining residues after the cone calorimeter test a) EVA/HA, b) EVA/HA-CNT, c) EVA/APP d) EVA/APP/HA, and e) EVA/APP/HA-CNT.

thanks to the formation of homogenous char layer (Fig. 11).

Total Smoke Production (TSP) curves are shown in Fig. 10 and the final TSP values are summarized in Table 3. From the results presented can be understood that TSP value was increased in the presence of APP. It may be related to the degradation of char which has taken contribution from APP. On the other hand, combining APP with HA or HA-CNT decreased the TSP.

Fig. 11 shows the macroscopic digital photographs of the residues after cone calorimeter tests. The remaining residue of EVA containing HA or HA-CNT is 6% of initial mass. These powder-like residues do not show any cohesion and cannot display any efficient fire barrier role (Fig. 11a and b). In contrast, the incorporation of APP enabled for a promoting cohesive char layer formation, but it unfortunately collapsed at the end of the test. When APP was combined with HA and HA-CNT, the char layer got stronger and remained cohesive till the end of the test.

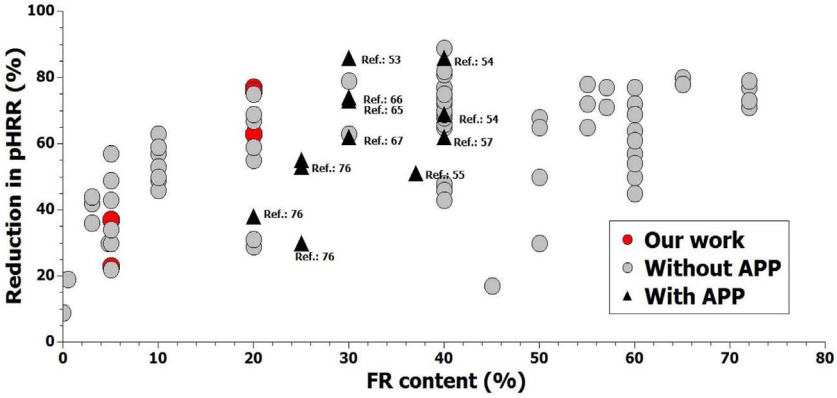

Fig. 12. A master curve on the extent of reduction in pHRR as a function of flame retardant content for 105 formulations (the corresponding reference for formulation "with APP" is indicated behind each point) [66,67].

3.3. Meta-analysis

In order to recognize the performance of the flame retardant systems developed for EVA, more than 30 research papers (105 formulations, Annex 1) were considered for comparison of the results of this work with other flame retardant systems previously addressed in the literature. From these research works, two values were extracted: reduction in pHRR (in comparison with pure EVA) and flame retardant (FR) content. Fig. 12 patterns the reduction in pHRR as a function of FR content (wt.%) for diverse formulations based on EVA as a master curve. It should be emphasized that this comparison does not account for grades of EVA and FR as well as external heat flux, which might be different from one work to the other, but still it provides a global view of the efficiency of the systems developed in the current report. As a whole, it can be recognized that reduction in pHRR tends to increase upon increasing FR content up to 30–40 wt.%. Above this threshold, the reduction in pHRR remains almost constant around 80% for the most effective formulations. Systems based on APP were used at loading levels ranging from 10 to 40 wt.%. It is evident from the master curve that fall in pHRR reached 87% by combining APP (20 wt.%) and hexakis(dodecylamino)cyclotriphosphazene (20 wt.%) [54]. Other formulations also led to a high decrease in pHRR (around 80%) at 30 wt.% of loading such as APP/4-(5,5-dimethyl-2-oxo-1,3,2-dioxaphosphorinan-2-yloxymethyl)-2,6,7-trioxa-1-phospha-bicyclo [2.2.2]octane-1-oxide (MOPO) [53] and APP/Triazine-based charring agent poly(4,6-dichloro-N-hydroxyethyl-1,3,5-triazin-2-amine-1,6-diaminohexane) [12]. It can be observed that the performances of our formulations are high with a pHRR reduction up to 78% for a moderate FR content: 20 wt.%.

4. Conclusion

In this study, hydroxyapatite (HA) and a physical blend of HA and multi-walled carbon nanotube (HA-CNT) were applied as flame retardant for EVA. The assigned ingredients were melt-blended with EVA to make a flame retardant nanocomposite. Thermal stability and flame retardancy of the obtained composites were investigated using TGA and cone calorimeter tests. It was revealed that the incorporation of 5 wt.% of HA-CNT causes a reduction of ca. 37% in pHRR, which appears promising compared to the available data in such systems. The best results in terms of reduction in pHRR were when HA or HA-CNT (5 wt.%) were combined with APP (15 wt.%). In a particular manner, the combination of HA-CNT and APP ended in a promising formulation with excellent flame retardancy. The EVA/APP/HA-CNT sample showed the lowest HRR during the first 400 s and avoided a sharp increase of HRR at the end of the test. The "meta-analysis" of the literature available on flame retardancy of EVA showed that the studied systems in the present work lies in an acceptable place, relatively on the top of the EVA-based flame retardant systems with efficient performance.

Acknowledgements

The authors wish to thank the technological platform "Plastinnov" at the University of Lorraine for their support in the preparation of samples and fire tests.

Appendix A. Collected data from the literature on "Flame retardancy of EVA".

N°	Wt.% FR	Name(s) of Flame retardant(s), incorporated into EVA	Reduction in pHRR (%)	Ref.
	20	APP/HA-CNT	77	our paper
1	40	Hexakis(dodecylamino)cyclotriphosphazene 20/APP10/Trimer10	86	[54]
2	40	Hexakis(dodecylamino)cyclotriphosphazene 17.5/APP17.5/Trimer5	64	[54]
3	40	Hexakis(dodecylamino)cyclotriphosphazene 20/APP20	87	[54]
4	37	APP/PER/TAIC	53	[55]
5	15	DNA	36	[56]
6	40	Cyclodextrin microencapsulated ammonium polyphosphate	69	[57]
7	40	Cyclodextrin/ammonium polyphosphate	61	[58]
8	30	APP/4-(5,5-dimethyl-2-oxo-1,3,2-dioxaphosphorinan-2-yloxymethyl)- 2,6,7-trioxa-1-phospha-bicyclo [2.2.2]octane-1-oxide	86	[53]
9	10	ZnAl–borate LDH	63	[58]
10	3	MgAl–borate LDH	42	[58]
11	5	MgAl–borate LDH	43	[58]
12	10	MgAl–borate LDH	49	[58]

13	20	MgAl–borate LDH	55	[58]
14	40	MgAl–borate LDH	74	[58]
15	3	ZnAl–borate LDH	36	[58]
16	5	ZnAl–borate LDH	57	[58]
17	20	ZnAl–borate LDH	59	[58]
18	40	ZnAl–borate LDH	77	[58]
19	40	Magnesium hydroxide (MDH)	65	[58]
20	40	Aluminum trihydroxide (ATH)	89	[58]
21	40	Zinc borate	89	[58]
22	40	Zinc hydroxide	47	[58]
23	40	MDH/ATH	72	[58]
24	40	Zinc hydroxide/ATH	48	[58]
25	10	ZnAl–borate/melamine polyphosphate	53	[58]
26	10	Melamine polyphosphate	60	[58]
27	10	Phenyl phosphonate-intercalated MgAl–LDH, melamine polyphosphate, and boric acid	60	[59]
28	10	Boric acid	46	[59]
29	10	Melamine polyphosphate	57	[59]
30	10	MgAl-PPh	53	[59]
31	4.76	Dimethyl-dioctadecylammoniumtreated MMT	30	[44]
32	2	Zr phosphate	14	[60]
33	30	expanded graphite	79	[61]
34	30	graphite oxide	63	[61]
35	6	Silicon and phosphorus	35	[62]
36	10	MMT	50	[14]
37	60	$Mg(OH)_2$	57	[63]
38	60	$Ca(OH)_2$	50	[63]
39	60	$Ca(OH)_2{\cdot}Mg(OH)_2{\cdot}MgO$	54	[63]
40	60	$Ca(OH)_2{\cdot}Mg(OH)_2$	77	[63]
41	55	MDH	65	[64]
42	55	MDH and hollow glass microspheres	78	[64]
43	55	MDH and hollow glass microspheres	72	[64]
44	57	ATH and melamine borate	77	[65]
45	57	ATH	71	[65]
46	57	ATH-MP	76	[65]
47	57	ATH- Melamine (MEL)	77	[65]
48	30	APP/poly(piperazinyl succinamide)	74	[65]
49	30	APP	51	[65]
50	30	APP/poly(piperazinyl malonamide)	50	[65]
51	30	APP/charring agent	62	[65]
52	30	Triazine-based charring agent poly(4,6-dichloro-N-hydroxyethyl-1,3,5-triazin-2-amine-1,6-diaminohexane) with ammonium polyphosphate	73	[12]
53	20	dodecylsulfate (DDS) intercalated and surface uptaken nano-LDHs containing Ni	75	[68]
54	20	DDS-NiAl-CO_3	67	[68]
55	20	NiAl–CO_3	69	[68]
56	5	A phosphorus nitrogen containing compound, N-(2-(5,5-dimethyl-1,3,2-dioxaphosphinyl-2-ylamino)-hexylacetamide-2-propyl acid (PAHPA)-LDHs	43	[69]
57	5	PAHPA	25	[69]
58	5	LDHs	30	[69]
59	5	PAHPA/LDHs	34	[69]
60	10	Cloisite30B	59	[14]
61	3	Cloisite30B	44	[14]
62	5	Cloisite30B	49	[14]
63	5	Na + 5	22	[14]
64	0.025	MWCNT	9	[70]
65	0.5	MWCNT	19	[70]
66	60	ATH 60 wt.%	72	[15]
67	60	ATH 40 wt.%/Melamine 20 wt.%	45	[15]
68	60	ATH 20 wt.%/Melamine 40 wt.%	20	[15]
69	65	ATH	80	[71]
70	50	MDH	30	[72]
71	50	MDH/MWNT1	50	[72]
72	50	MDH/MWNT2	68	[72]
73	50	MDH/MWNT3	65	[72]
74	72	ATH	71	[65]
75	72	ATH-MEL (5:1)	77	[65]
76	72	ATH-MEL (10:1)	79	[65]

77	72	ATH-MEL (25:1)	73	[65]
78	65	ATH	78	[73]
79	40	ATH	72	[74]
80	40	ATH	74	[74]
81	40	ATH	66	[74]
82	40	ATH	74	[74]
83	40	ATH	68	[74]
84	40	ATH	69	[74]
85	40	ATH	66	[74]
86	40	ATH	65	[74]
87	40	ATH/DIATOM	70	[74]
88	40	ATH/DIATOM	73	[74]
89	40	ATH/DIATOM	75	[74]
90	40	ATH/DIATOM	81	[74]
91	40	ATH/DIATOM	82	[74]
92	45	DIATOM	17	[74]
93	20	ATH	29	[74]
94	20	ATH/Silica	31	[74]
95	40	ATH	46	[74]
96	40	ATH/Silica	43	[74]
97	60	ATH	64	[74]
98	60	ATH/Silica	64	[74]
99	60	MDH	69	[74]
100	60	MDH/Silica	61	[74]
101	40	APP	62	[75]
102	20	APP	38	[76]
103	25	APP	30	[76]
104	25	APP20/Nanodiamond D5	55	[76]
105	25	APP20/Nanodiamond −P5	53	[76]

References

[1] E.D. Weil, Fire-protective and flame-retardant coatings—a state-of-the-art review, J. Fire Sci 29 (2011) 259–296.
[2] N.K. Saxena, D.R. Gupta, Development and evaluation of fire retardant coatings, Fire Technol. 26 (1990) 329–341.
[3] A.M. Henderson, Ethylene-vinyl acetate (EVA) copolymers: a general review, IEEE Electr. Insul. Mag 9 (1993) 30–38.
[4] Global Ethylene Vinyl Acetate Market 2016–2020, http://www.researchandmarkets.com, June (2016).
[5] R. Liang, P. Zhang, C. Wei, H. Li, Z. Wang, X. Huang, W. Yin, X. Chen, Spontaneous formation of bimodal particle size distributions: a novel one-step strategy for obtaining high solid content low viscosity poly(vinyl acetate-co-ethylene) latexes, Prog. Org. Coat. 110 (2017) 86–96.
[6] S.P. Tambe, S.K. Singh, M. Patri, D. Kumar, Effect of pigmentation on mechanical and anticorrosive properties of thermally sprayable EVA and EVAl coatings, Prog. Org. Coat. 72 (2011) 315–320.
[7] British Standard BS EN 50200, Method of Test for Resistance to Fire of Unprotected Small Cables for Use in Emergency Circuits, British Standard Institution, 2006.
[8] S. Hamdani-Devarennes, A. Pommier, C. Longuet, J.-M. Lopez-Cuesta, F. Ganachaud, Calcium and aluminium-based fillers as flame-retardant additives in silicone matrices II. Analyses on composite residues from an industrial-based pyrolysis test, Polym. Degrad. Stab. 96 (2011) 1562–1572.
[9] B.K. Kandola, P. Luangtriratana, S. Duquesne, S. Bourbigot, The effects of thermophysical properties and environmental conditions on fire performance of intumescent coatings on glass fibre-reinforced epoxy composites, Materials 8 (2015) 5216–5237.
[10] L. Calabrese, F. Bozzoli, G. Bochicchio, B. Tessadri, S. Rainieri, G. Pagliarini, Thermal characterization of intumescent fire retardant paints, J. Phys. Conf. Ser 547 (2014) 012005.
[11] A. Riva, G. Camino, L. Fomperie, P. Amigouet, Fire retardant mechanism in intumescent ethylene vinyl acetate compositions, Polym. Degrad. Stab. 82 (2003) 341–346.
[12] C. Feng, M. Liang, J. Jiang, H. Liu, J. Huang, Synergistic effect of ammonium polyphosphate and triazine-based charring agent on the flame retardancy and combustion behavior of ethylene-vinyl acetate copolymer, J. Anal. Appl. Pyrolysis 119 (2016) 259–269.
[13] A. Szép, A. Szabó, N. Tóth, P. Anna, G. Marosi, Role of montmorillonite in flame retardancy of ethylene-vinyl acetate copolymer, Polym. Degrad. Stab. 91 (2006) 593–599.
[14] S. Duquesne, C. Jama, M. Le Bras, R. Delobel, P. Recourt, J. Gloaguen, Elaboration of EVA-nanoclay systems—characterization, thermal behaviour and fire performance, Compos. Sci. Technol. 63 (2003) 1141–1148.
[15] J. Zilberman, T.R. Hull, D. Price, G.J. Milnes, F. Keen, Flame retardancy of some ethylene-vinyl acetate copolymer-based formulations, Fire Mater. 24 (3) (2000) 159–164.
[16] G. Camino, R. Sgobbi, A. Zaopo, S. Colombier, C. Scelza, Investigation of flame retardancy in EVA, Fire Mater. 24 (2000) 85–90.
[17] T. McNally, P. Pötschke, Polymer-carbon Nanotube Composites: Preparation, Properties and Applications, Elsevier, 2011.
[18] M. Batistella, B. Otazaghine, R. Sonnier, A.-S. Caro-Bretelle, C. Petter, J.-M. Lopez-Cuesta, Fire retardancy of ethylene vinyl acetate/ultrafine kaolinite composites, Polym. Degrad. Stab. 100 (2014) 54–62.
[19] D. Gnanasekaran, P.H. Massinga, W.W. Focke, A detailed review on behavior of ethylene-vinyl acetate copolymer nanocomposite materials, Materials Behavior: Research Methodology and Mathematical Models, Apple Academic Press, 2015, pp. 89–123.
[20] M. Cross, P. Cusack, P. Hornsby, Effects of tin additives on the flammability and smoke emission characteristics of halogen-free ethylene-vinyl acetate copolymer, Polym. Degrad. Stab. 79 (2003) 309–318.
[21] L. Clerc, L. Ferry, E. Leroy, J.-M. Lopez-Cuesta, Influence of talc physical properties on the fire retarding behaviour of (ethylene-vinyl acetate copolymer/magnesium hydroxide/talc) composites, Polym. Degrad. Stab. 88 (2005) 504–511.
[22] M. Zanetti, T. Kashiwagi, L. Falqui, G. Camino, Cone calorimeter combustion and gasification studies of polymer layered silicate nanocomposites, Chem. Mater. 14 (2002) 881–887.
[23] Y. Arao, Flame retardancy of polymer nanocomposite, Paper Presented At: Flame Retardants (2015).
[24] M. Muller, S. Bourbigot, S. Duquesne, R.A. Klein, G. Giannini, C.I. Lindsay, Measurement and investigation of intumescent char strength: application to polyurethanes, J. Fire Sci. 31 (2013) 293–308.
[25] T. Mariappan, Recent developments of intumescent fire protection coatings for structural steel: a review, J. Fire Sci. 34 (2016) 120–163.
[26] D. Yi, R. Yang, C.A. Wilkie, Full scale nanocomposites: clay in fire retardant and polymer, Polym. Degrad. Stab. 105 (2014) 31–41.
[27] M. Entezam, H.A. Khonakdar, S.M.A. Jafari, S. Raji, M. Otadi, Thermal stability and flammability of ethylene vinyl acetate copolymers in presence of nanoclay and a halogen-free flame retardant, J. Vinyl Add. Tech. (2016).
[28] N. Zaharri, N. Othman, Z.M. Ishak, Thermal and mechanical properties of zeolite filled ethylene vinyl acetate composites, Procedia Chem. 4 (2012) 95–100.
[29] Y. Zhang, R.-q. Peng, Z.-p. Fang, X.-n. Li, Flammability characterization and effects of magnesium oxide in halogen-free flame-retardant EVA blends, Chin. J. Polym. Sci. 33 (2015) 1683–1690.
[30] X.-y. Pang, M.-q. Weng, Preparation of expandable graphite composite under the auxiliary intercalation of Zinc sulfate and its flame retardancy for ethylene/vinyl acetate copolymer, Int. J. ChemTech Res. 6 (2014) 1291–1298.
[31] X. Wu, L. Wang, C. Wu, G. Wang, P. Jiang, Flammability of EVA/IFR (APP/PER/ZB

system) and EVA/IFR/synergist (CaCO3, NG, and EG) composites, J. Appl. Polym. Sci. 126 (2012) 1917–1928.
[32] L. Li, Y. Qian, C. Jiao, Synergistic flame retardant effects of ammonium polyphosphate in ethylene-vinyl acetate/layered double hydroxides composites, Polym. Eng. Sci. 54 (2014) 766–776.
[33] S. Elbasuney, H.E. Mostafa, Synthesis and surface modification of nanophosphorous-based flame retardant agent by continuous flow hydrothermal synthesis, Particuology 22 (2015) 82–88.
[34] Q.X. Dong, Q.J. Chen, W. Yang, Y.L. Zheng, X. Liu, Y.L. Li, M.B. Yang, Thermal properties and flame retardancy of polycarbonate/hydroxyapatite nanocomposite, J. Appl. Polym. Sci. 109 (2008) 659–663.
[35] B. Dholakiya, Use of non-traditional fillers to reduce flammability of polyester resin composites, Polimeri 30 (2009) 10–17.
[36] S. Velayudhan, P. Ramesh, H. Varma, K. Friedrich, Dynamic mechanical properties of hydroxyapatite-ethylene vinyl acetate copolymer composites, Mater. Chem. Phys. 89 (2005) 454–460.
[37] S. Zhou, L. Zhang, Y.-Y. Wang, Y. Zuo, S.-B. Gao, Y.-B. Li, Fabrication of hydroxyapatite/ethylene-vinyl acetate/polyamide 66 composite scaffolds by the injection-molding method, Polym. Plast. Technol. Eng. 50 (2011) 1047–1054.
[38] Y. Wang, L. Zhang, S. Zhou, D. Huang, Y. Morsi, S. Gao, M. Gong, Y. Li, Investigation of nonisothermal crystallization of hydroxyapatite/ethylene-vinyl acetate (HA/EVA) composite, J. Appl. Polym. Sci. 122 (2011) 1412–1419.
[39] G. Xu, J. Cheng, H. Wu, Z. Lin, Y. Zhang, H. Wang, Functionalized carbon nanotubes with oligomeric intumescent flame retardant for reducing the agglomeration and flammability of poly (ethylene vinyl acetate) nanocomposites, Polym. Compos. 34 (2013) 109–121.
[40] L. Wang, P.K. Jiang, Thermal and flame retardant properties of ethylene-vinyl acetate copolymer/modified multiwalled carbon nanotube composites, J. Appl. Polym. Sci. 119 (2011) 2974–2983.
[41] L. Wang, J. Yu, Z. Tang, P. Jiang, Synthesis, characteristic, and flammability of modified carbon nanotube/poly (ethylene-co-vinyl acetate) nanocomposites containing phosphorus and silicon, J. Mater. Sci. 45 (2010) 6668–6676.
[42] M.C. Costache, M.J. Heidecker, E. Manias, G. Camino, A. Frache, G. Beyer, R.K. Gupta, C.A. Wilkie, The influence of carbon nanotubes, organically modified montmorillonites and layered double hydroxides on the thermal degradation and fire retardancy of polyethylene, ethylene-vinyl acetate copolymer and polystyrene, Polymer 48 (2007) 6532–6545.
[43] S. Peeterbroeck, F. Laoutid, B. Swoboda, J.M. Lopez-Cuesta, N. Moreau, J.B. Nagy, M. Alexandre, P. Dubois, How carbon nanotube crushing can improve flame retardant behaviour in polymer nanocomposites? Macromol. Rapid Commun. 28 (2007) 260–264.
[44] G. Beyer, Short communication: carbon nanotubes as flame retardants for polymers, Fire Mater. 26 (2002) 291–293.
[45] JCPDS File No. 9-432, International Center for Diffraction Data.
[46] F. Gholami, S. Ismail, A.F.M. Noor, Development of carboxylated multi-walled carbon nanotubes and bovine serum albumin reinforced hydroxyapatite for bone substitute applications, J. Aust. Ceram. Soc. (2017) 1–11.
[47] R.B. Wang, W.J. Weng, X.L. Deng, K. Cheng, X.G. Liu, P.Y. Du, G. Shen, G.R. Han, Dissolution behavior of submicron biphasic tricalcium phosphate powders, Key Eng. Mater. Trans Tech Publ, 2006, pp. 223–226.
[48] W. Janusz, E. Skwarek, S. Pasieczna-Patkowska, A. Slosarczyk, Z. Paszkiewicz, A. Rapacz-Kmita, A study of surface properties of calcium phosphate by means of photoacoustic spectroscopy (FT-IR/PAS), potentiometric titration and electrophoretic measurements, Eur. Phys. J. Spec. Top. 154 (2008) 329–333.
[49] S.P. Victor, T.S. Kumar, Processing and properties of injectable porous apatitic cements, J. Ceram. Soc. Jpn. 116 (2008) 105–107.
[50] M. Tahriri, M. Solati-Hashjin, H. Eslami, Synthesis and characterization of hydroxyapatite nanocrystals via chemical precipitation technique, Iran. J. Pharm. Sci. 4 (2008) 127–134.
[51] D.N. Ungureanu, N. Angelescu, Z. Bacinschi, E.V. Stoian, C.Z. Rizescu, Thermal stability of chemically precipitated hydroxyapatite nanopowders, Int. J. Biol. Biomed. Eng. 5 (2011) 57–64.
[52] F. Laoutid, L. Bonnaud, M. Alexandre, J.-M. Lopez-Cuesta, P. Dubois, New prospects in flame retardant polymer materials: from fundamentals to nanocomposites, Mater. Sci. Eng. R: Rep. 63 (2009) 100–125.
[53] D.-Y. Wang, X.-X. Cai, M.-H. Qu, Y. Liu, J.-S. Wang, Y.-Z. Wang, Preparation and flammability of a novel intumescent flame-retardant poly (ethylene-co-vinyl acetate) system, Polym. Degrad. Stab. 93 (2008) 2186–2192.
[54] C. Wu, W. Wu, H. Qu, J. Xu, Synthesis of a novel phosphazene derivative and its application in intumescent flame retardant–EVA copolymer composites, Mater. Lett. 160 (2015) 282–285.
[55] B. Wang, X. Wang, Y. Shi, G. Tang, Q. Tang, L. Song, Y. Hu, Effect of vinyl acetate content and electron beam irradiation on the flame retardancy, mechanical and thermal properties of intumescent flame retardant ethylene-vinyl acetate copolymer, Radiat. Phys. Chem. 81 (2012) 308–315.
[56] J. Alongi, A. Di Blasio, F. Cuttica, F. Carosio, G. Malucelli, Bulk or surface treatments of ethylene vinyl acetate copolymers with DNA: investigation on the flame retardant properties, Eur. Polym. J. 51 (2014) 112–119.
[57] B. Wang, X. Qian, Y. Shi, B. Yu, N. Hong, L. Song, Y. Hu, Cyclodextrin microencapsulated ammonium polyphosphate: preparation and its performance on the thermal, flame retardancy and mechanical properties of ethylene vinyl acetate copolymer, Compos. Part B: Eng. 69 (2015) 22–30.
[58] C. Nyambo, C.A. Wilkie, Layered double hydroxides intercalated with borate anions: fire and thermal properties in ethylene vinyl acetate copolymer, Polym. Degrad. Stab. 94 (2009) 506–512.
[59] C. Nyambo, E. Kandare, C.A. Wilkie, Thermal stability and flammability characteristics of ethylene vinyl acetate (EVA) composites blended with a phenyl phosphonate-intercalated layered double hydroxide (LDH), melamine polyphosphate and/or boric acid, Polym. Degrad. Stab. 94 (2009) 513–520.
[60] J. Alongi, A. Frache, Flame retardancy properties of α-zirconium phosphate based composites, Polym. Degrad. Stab. 95 (2010) 1928–1933.
[61] X. Wu, L. Wang, C. Wu, J. Yu, L. Xie, G. Wang, P. Jiang, Influence of char residues on flammability of EVA/EG, EVA/NG and EVA/GO composites, Polym. Degrad. Stab. 97 (2012) 54–63.
[62] J. Bonnet, V. Bounor-Legaré, F. Boisson, F. Mélis, G. Camino, P. Cassagnau, Phosphorus based organic–inorganic hybrid materials prepared by reactive processing for EVA fire retardancy, Polym. Degrad. Stab. 97 (2012) 513–522.
[63] F. Laoutid, M. Lorgouilloux, D. Lesueur, L. Bonnaud, P. Dubois, Calcium-based hydrated minerals: promising halogen-free flame retardant and fire resistant additives for polyethylene and ethylene vinyl acetate copolymers, Polym. Degrad. Stab. 98 (2013) 1617–1625.
[64] L. Liu, J. Hu, J. Zhuo, C. Jiao, X. Chen, S. Li, Synergistic flame retardant effects between hollow glass microspheres and magnesium hydroxide in ethylene-vinyl acetate composites, Polym. Degrad. Stab. 104 (2014) 87–94.
[65] C. Hoffendahl, G. Fontaine, S. Duquesne, F. Taschner, M. Mezger, S. Bourbigot, The combination of aluminum trihydroxide (ATH) and melamine borate (MB) as fire retardant additives for elastomeric ethylene vinyl acetate (EVA), Polym. Degrad. Stab. 115 (2015) 77–88.
[66] L.-P. Dong, C. Deng, Y.-Z. Wang, Influence of small difference in structure of polyamide charring agents on their flame-retardant efficiency in EVA, Polym. Degrad. Stab. 135 (2017) 130–139.
[67] C. Feng, M. Liang, W. Chen, J. Huang, H. Liu, Flame retardancy and thermal degradation of intumescent flame retardant EVA composite with efficient charring agent, J. Anal. Appl. Pyrolysis 113 (2015) 266–273.
[68] L. Wang, B. Li, X. Zhang, C. Chen, F. Zhang, Effect of intercalated anions on the performance of Ni–Al LDH nanofiller of ethylene vinyl acetate composites, Appl. Clay Sci. 56 (2012) 110–119.
[69] G. Huang, Z. Fei, X. Chen, F. Qiu, X. Wang, J. Gao, Functionalization of layered double hydroxides by intumescent flame retardant: preparation, characterization, and application in ethylene vinyl acetate copolymer, Appl. Surf. Sci. 258 (2012) 10115–10122.
[70] G. Beyer, Polymer–carbon Nanotube Composites for Flame-retardant Cable Applications, Woodhead Publishing Limited, 2011.
[71] F.-E. Ngohang, G. Fontaine, L. Gay, S. Bourbigot, Smoke composition using MLC/FTIR/ELPI: application to flame retarded ethylene vinyl acetate, Polym. Degrad. Stab. 115 (2015) 89–109.
[72] L. Ye, Q. Wu, B. Qu, Synergistic effects and mechanism of multiwalled carbon nanotubes with magnesium hydroxide in halogen-free flame retardant EVA/MH/MWNT nanocomposites, Polym. Degrad. Stab. 94 (2009) 751–756.
[73] F. Ngohang, G. Fontaine, L. Gay, S. Bourbigot, Revisited investigation of fire behavior of ethylene vinyl acetate/aluminum trihydroxide using a combination of mass loss cone, fourier transform infrared spectroscopy and electrical low pressure impactor, Polym. Degrad. Stab. 106 (2014) 26–35.
[74] F. Cavodeau, R. Sonnier, B. Otazaghine, J.-M. Lopez-Cuesta, C. Delaite, Ethylene-vinyl acetate copolymer/aluminium trihydroxide composites: a new method to predict the barrier effect during cone calorimeter tests, Polym. Degrad. Stab. 120 (2015) 23–31.
[75] C. Siat, M. Le Bras, S. Bourbigot, Combustion behaviour of ethylene vinyl acetate copolymer–based intumescent formulations using oxygen consumption calorimetry, Fire Mater. 22 (1998) 119–128.
[76] C. Presti, L. Ferry, J.G. Alauzun, L. Dumazert, B. Gallard, J.-C. Quantin, J.-M.L. Cuesta, P.H. Mutin, Functionalized nanodiamond as potential synergist in flame-retardant ethylene vinyl acetate, Diamond Relat. Mater. 76 (2017) 141–149.